scientific reports

Check for updates

OPEN

Process and mechanism modeling of cefotaxime removal from hospital wastewater using pistachio shells based magnetic activated carbon nanoparticles

Atefeh Rahmani[1], Haripriya Naidu[2], Tomasz Świergosz[3], Hamid Reza Rahimi[4], Zahra Mousavi[1], Maryam Dolatabadi[5]✉ & Saeid Ahmadzadeh[6,7]✉

Antibiotic residues have been extensively identified in diverse aquatic environments, posing significant health risks to both humans and animals, while also presenting challenges to the environment. Consequently, the imperative need to effectively removal antibiotics from the environment has become a very importance issue. In this study, response surface methodology with central composite design was employed to systematically investigate the effects of key process parameters, on the removal of cefotaxime (CTX) from hospital wastewater using pistachio sells based activated carbon modified with $FeCl_3$. The modified activated carbon was synthesized using a thermochemical method and characterized by analytical techniques including FE-SEM, FTIR, XRD, pH_{pzc}, and BET analysis, which demonstrated its remarkable physicochemical properties. Maximum removal efficiency of 99.1% was obtained via the optimal values of 45 mg L^{-1} of initial CTX concentration, solution pH 7, and 200 mg L^{-1} of Fe@ACP dosage, 56 min of reaction time through adsorption process. According to the results, the non-linear Langmuir isotherm model ($R^2 = 0.9931$) and non-linear second order kinetic model ($R^2 = 0.9934$) are suitably described the monolayer and chemisorption of CTX adsorption. The maximum adsorption capacity of Fe@ACP is 651.6 mg g^{-1}. Consequently, the developed treatment process revealed successful performance for quick and efficient removal of CTX by Fe@ACP. The developed process introduced an economic and green approach for the comprehensive utilization of agricultural waste resources used for environmental pollution control.

Keywords Adsorption, Pharmaceutical compound, Response surface methodology, Isotherms, Kinetics

Water is a vital necessity for the sustenance of all living organisms. However, with the increase in industrialization, water quality has been significantly impacted by the release of harmful pollutants into the environment[1]. In recent years, personal care products (PCPs) and pharmaceuticals have become increasingly recognized as one class of water pollutants, owing to their widespread usage on a global scale[2]. These compounds are also known to have unknown biological and eco-toxicological effects. Pharmaceuticals or drugs contain a wide range of compounds that are used to treat health problems in living beings. Among these compounds, antibiotics are commonly utilized for the treat and control of bacterial infections. The administration of specific antibiotics to both animals and humans plays a pivotal role in effectively treating a wide range of bacterial diseases, leading to

[1]Department of Pharmacology and Toxicology, Faculty of Pharmacy, Pharmaceutical Sciences Branch, Islamic Azad University, Tehran, Iran. [2]Graduated from Department of Civil Engineering, Kansas State University, Fiedler Hall, 1701C Platt Street, Manhattan, KS 66502, USA. [3]Department of Chemical Technology and Environmental Analysis, Faculty of Chemical Engineering and Technology, Cracow University of Technology, 24 Warszawska St, Kraków 31-155, Poland. [4]Department of Toxicology and Pharmacology, faculty of Pharmacy, Kerman University of Medical Sciences, Kerman, Iran. [5]Environmental Health Engineering Research Center, Kerman University of Medical Sciences, Kerman, Iran. [6]Pharmaceutics Research Center, Institute of Neuropharmacology, Kerman University of Medical Sciences, Kerman, Iran. [7]Pharmaceutical Sciences and Cosmetic Products Research Center, Kerman University of Medical Sciences, Kerman, Iran. ✉email: health.dolatabadi@gmail.com; saeid.ahmadzadeh@kmu.ac.ir; chem_ahmadzadeh@yahoo.com

a significant enhancement in the overall life expectancy[3,4]. Nevertheless, the widespread use of antibiotics has resulted in the accumulation of minute quantities of these compounds in aquatic ecosystems. The predominant origins of these pollutants can be ascribed to a range of wastewater sources, encompassing pharmaceutical industries, hospitals, domestic environments, livestock farming, and surface runoff[5]. In conventional wastewater treatment facilities, antibiotics are not entirely eliminated. In addition, the biological organisms employed in the biological treatment processes are continuously exposed to sub-therapeutic concentrations[6]. As a result, the selective pressure exerted contributes to the emergence of antibiotic-resistant bacteria[7,8]. The estimated annual mortality resulting from antibiotic resistance exceeds 23,000 individuals in the United States and Europe combined. The WHO has categorized antimicrobial resistance as a public health threat in 2015[9]. So far, various antibiotics such as ciprofloxacin, sulfamethoxazole, tetracycline, azithromycin, etc. have been detected in different concentrations in wastewater and water sources[10,11].

Cefotaxime (CTX), an antibiotic belonging to the β-lactam class, is frequently employed in the treatment of pulmonary and urinary tract ailments. This particular antibiotic exhibits significant effectiveness against a diverse spectrum of bacteria[12]. Concentrations of over 0.2 μg L^{-1} of CTX have been detected in the effluent of wastewater treatment plants[13]. Multiple research studies have identified the presence of CTX within various aqueous matrices, such as hospital wastewater and wastewater treatment plants, with recorded concentrations ranging from 0.30 ng L^{-1} to 18 μg L^{-1}[14]. In the wastewater facility situated within a pharmaceutical manufacturing park in China, the measured concentrations of CTX in the incoming feed were found to be 18.08 ± 4.02 μg L^{-1}, whereas in the outlet of the facility, the concentrations were determined to be 0.55 ± 0.62 μg L^{-1}[15,16]. The detection of CTX in the effluents of wastewater indicates that conventional wastewater treatment methods are inadequate for its removal. Several studies have been conducted on the removal of antibiotics from aqueous media by methods such as adsorption[17,18], biochemical degradation[19], chemical oxidation[20], electrochemical degradation, and photochemical degradation[21–24]. Among these methods, adsorption technology has been established as a low cost and environmentally friendly method[1,25]. Several advantages of this technology such as high removal capacity, minimal space requirements, simple operation, and ability to recycle the adsorbent material make this a suitable method for the removal of antibiotics from polluted water[26,27]. The efficacy of an adsorption process in removing contaminants is contingent upon the specific attributes of the adsorbent material employed, as well as the composition of the wastewater undergoing treatment. In this method, materials characterized by a substantial surface area and extreme porosity, such as activated carbon (AC), are frequently utilized[28,29]. Various carbonaceous materials, including plant-based materials and coal, are utilized in the generation of activated carbon (AC).

The application of AC obtained from coal is hindered by its high price and difficult regeneration process. However, AC obtained from agricultural residues, industrial wastes, and municipal wastes are low-cost alternatives. Several studies have been conducted on the improvement of removal efficiency of contaminants by adsorbents using modifications in physicochemical properties of AC, for example, using chemical compounds such as diethylenetriamine, ammonia, and sulfonic acid to modify AC to remove phenol[30], 2, 4-dichlorophenol[31], and cationic dyes[32], respectively. In this study, the activated carbon originated from the agriculture waste materials of pistachio farms. Due to the high production quantity of pistachio in Iran, its shell was candidate as an attractive adsorbent of low cost, abundant, and renewable material for treatment process. Moreover, the AC obtained from pistachio wood shell (ACP) modified to enhance its adsorption characteristics for the CTX removal from aqueous media. The pistachio wood shells were activated using ferric chloride ($FeCl_3$). The characterization of the synthesized adsorbent was carried out by pH point of zero charge (pH_{pzc}), X-Ray diffraction (XRD), Brunauer-Emmett-Teller (BET), Fourier-transform infrared spectroscopy (FTIR), and analysis field emission scanning electron microscopes (FE-SEM). In addition, the influence of parameters such as initial concentration of CTX, solution pH, adsorbent dosage, and equilibration time were investigated to increase the understanding of CTX adsorption properties onto the modified AC. A statistical analysis employing central composite design (CCD) was employed to develop and investigate the mathematical model. The adsorption characteristics and mechanism were elucidated through the examination of adsorption isotherms and kinetic studies.

Materials and methods

Chemicals

Cefotaxime ($C_{16}H_{17}N_5O_7S_2$), acetonitrile HPLC grade (CH_3CN), propan-2-one (CH_3-CO-CH_3), methanol (CH_3OH), ferric chloride ($FeCl_3$), formic acid (HCOOH), hydrochloric acid (HCl), phosphoric acid (H_3PO_4), sulfuric acid (H_2SO_4), nitric acid (HNO_3), sodium chloride (NaCl), sodium hydroxide (NaOH), standard activated carbon (SAC), and trifluoroacetic acid (CF_3COOH) were purchased from Merck® (Germany). Double distilled water (DDW) obtained from (Abban, Iran) was used to prepare the solutions. The batch adsorption equilibrium tests were conducted using Erlenmeyer flasks (working volume of 100 mL) and were kept for mixing on a shaker incubator (Heidolph-Unimax 1010, Germany).

Preparation of adsorbent

The source material used for synthesizing activated carbon (AC) was obtained from pistachio shells acquired from a local farm in Kerman, Iran. The pistachio shells were crushed and grinded in a (Electric mill, TOOS SHEKAN, TS1300) to < 0.5 mm particle size. Then the particles were several washed with DDW and dried at 105 °C for 1 h (Aven, Pars Azma, S.R 81). The dried shells particles were treated with phosphoric acid at a concentration of 0.5 M and at a weight/volume ratio of 1:100 (g mL^{-1} of shells particles: acid). These particles were then carbonized in an electrical furnace (Furnace, KSL1700X–H5) at 500 ± 5 °C for 1 h. Subsequently, the carbonized particles were subjected to heating at a rate of 10 °C min^{-1} until reaching a temperature of 850 ± 50 °C, while maintaining a N_2 flow rate of 0.05 L min^{-1}. When the temperature reached about 857 °C, Steam was also introduced into the furnace at a rate of 0.7 mL min^{-1} for 80 min. The carbonized particles were

left in the electrical furnace in the nitrogen atmosphere until the temperature reached to the room temperature. The cooled particles were sieved and washed with DDW until a constant pH was obtained. Then, the particles were filtered using Whatman™ cellulose filter papers (ashless, grade 40, United Kingdom) and dried at 110 ± 5 °C in (Aven, Pars Azma, S.R 81). The carbonized particles obtained from this procedure was named as AC from pistachio shells (ACP). These particles were then treated with HNO_3 for 3 h at 80 ± 5 °C to impart hydrophilicity. For modification of ACP was soaked in the 0.3 M of $FeCl_3$ solution. ACP to ranging between 0.5 and 5 g, per 100 mL $FeCl_3$ (0.3 M) were used. Each solution was agitated at ambient temperature (20 ± 2 °C) for 24 h. The modified activated carbon from pistachio shells (Fe@ACP) was prepared through a thermal treatment process in the presence of N_2 gas at a temperature of 800 ± 50 °C for 2 h[33].

Experimental design and analysis

The process design for an adsorption unit requires the optimization of several experimental parameters such as concentration of pollutants (adsorbate), dose of adsorbent, solution pH, equilibration time, temperature, adsorbent to adsorbate ratio, and etc. The response surface methodology (RSM) was utilized in this study to optimize the experimental parameters. The central composite design (CCD) utilized to identify the response pattern and establish a model based on four variables. Table 1 lists the ranges and levels of the experimental parameters used in the study.

Design Expert® (version 11) software was used to design the experiments. The analysis of variance (ANOVA) tools was employed to assess the significance of each individual experimental parameter (variables)as well as the developed of model. These tools also are studied Fischer's test value (*F*-value) and the probability value (*p*-value) at 95% confidence level. The accuracy and predictability of the models were studied using factors such as the R^2, adjusted R^2, predicted R^2, and plots such as normalized residue and adequate precision. The interactions between the experimental parameters and their effect of the response were studied using the contour plots and the response surface 3D plots[34]. The association between the experimental variables and the response was evaluated through the utilization of a quadratic polynomial response equation expressed in the following form:

$$Y = \beta_0 + \sum_{i=1}^{n} \beta_i X_i + \sum_{i=1}^{n} \beta_{ii} X_i^2 + \sum_{i=1}^{n-1} \sum_{j=i+1}^{n} \beta_{ij} X_i X_j + \epsilon \quad (1)$$

In the aforementioned equation, X_i and X_j represent the i^{th} and j^{th} independent variables, respectively, which exert an influence on the response. The regression constant is denoted by β_0, while β_i, β_{ii}, and β_{ij} represent the linear, quadratic, and interaction coefficients, respectively[35].

Adsorption experiments and characterization of adsorbents

Erlenmeyer flasks as reactors were used to conduct the batch experiments each using 100 mL test solution of CTX at various concentrations in the range of 10 to 150 mg L^{-1} and at room temperature (20 ± 2 °C). The pH levels of the solutions were adjusted by the addition of HCl and NaOH, while the monitoring of pH was performed using a pH meter (Metrohm 827 pH/mV). Then, adsorbents in the weight range of 50 to 250 mg L^{-1} were added to the reactors and kept for equilibration time in the range of 5 to 65 min at 150 rpm. Following the certain period of time, the mixture was centrifuged, and subsequently, the concentration of CTX in the solution was determined. The all experimental were replicated three times, and the mean value was recorded as the final result. The calculation of CTX removal efficiency was performed utilizing Eq. (2):

$$\text{CTX Removal } (\%) = \frac{\text{CTX}_0 - \text{CTX}_t}{\text{CTX}_0} \times 100 \quad (2)$$

In which CTX_0 and CTX_t (mg L^{-1}) represent the initial concentration and concentration at time t of CTX, respectively. The equilibrium adsorption capacity, q_e (mg g^{-1}), was determined by employing Eq. (3):

$$q_e = \frac{(\text{CTX}_0 - \text{CTX}_e) \times V}{W} \quad (3)$$

where, CTXe denotes the concentration of CTX at equilibrium (mg L^{-1}), V represents the volume of the working solution (L), and w corresponds to the weight of the adsorbent (g).

Coded variables (X_i)	Factors	Experimental field				
		−α	−1	0	+1	+α
X_1	A = Initial concentration of CTX (mg L^{-1})	10	45	80	115	150
X_2	B = Solution pH	3	5	7	9	11
X_3	C = Adsorbent dosage (Fe@ACP) (mg L^{-1})	50	100	150	200	250
X_4	D = Reaction time (min)	5	20	35	50	65

Table 1. Coded and actual values of the factors.

The HPLC system (Knauer, Berlin, Germany), C_{18} column (5 µm × 250 mm × 4.6 mm). A mobile phase of trifluoroacetic acid (5 mM, pH 3) and acetonitrile (70:30, v/v %) was used as a mobile phase in an isocratic mode (1.0 mL min^{-1}). The analyte, CTX, was detected at a wavelength of 235 nm[9].

The point of zero charge (pH_{pzc}) of the SAC, ACP, and Fe@ACP were determined using a pH meter (Metrohm 827 pH/mV). briefly, KNO_3 solution with 0.01 M concentration was used as electrolyte. The 50 mL of the electrolyte solution was added in several containers, after that the initial pH of each container was adjusted in the range of 2 to 12. In the next step, 250 mg of SAC, ACP, and Fe@ACP were added separately to the containers, and were shaken at 200 rpm for 24 h at ambient temperature. After 24 h, the pH of the solutions was measured, and the curve of initial pH was plotted against final pH for adsorbents. The intersection point of initial pH and final pH was introduced as pH at the pH_{pzc}[36].

Adsorption kinetics and isotherm models

The adsorption kinetic studies are needed to understand the dynamics of the process. The adsorption rate constants are important in the selection of adsorbent materials, as materials with high capacity and fast rates are desirable. In the field of kinetics, the first order, second order, and intra-particle diffusion (Weber-Morris) models are widely employed. In the first order model, the adsorption process is simplified by assuming that the solute diffuses through the liquid phase boundary. The adsorption rate in this model is proportional to the first state of contaminant concentration. The first order model has some limitations, as it does not give a good fit for the entire contact time. In the second order model, sorption is considered as the rate-controlling step and the adsorption capacity of the sorbent is considered[37]. In the experiments to determine kinetics, the CTX concentration of 80 mg L^{-1} at a pH of 6.5 and adsorbent dosage of 200 mg L^{-1} was used. The experiment was conducted for 60 min.

The study of adsorption isotherm is important for determining the adsorption capacity and needed to design the adsorption system. The CTX adsorption onto Fe@ACP was using Langmuir, Freundlich, and Sips isotherm models. The Langmuir isotherm model assumes that the adsorbent surface is uniform, the solute is adsorbed as a monolayer, no force between the solute molecules in the adsorbed state, and a dynamic equilibrium exists between the solute and the sorbent. On the other hand, the Freundlich isotherm model proposes the existence of a heterogeneous surface on the adsorbent material[13,14]. The adsorption equilibrium of CTX on Fe@ACP was modeled using non-linear equations of Langmuir, Freundlich, and Sips isotherm models by fitting experimental results to the models. The adsorption equilibrium experiments were conducted using a fixed dosage of adsorbent of 200 mg L^{-1} into a series of reactors containing solution of CTX in the concentration range of 25–125 mg L^{-1} with a pH of 6.5 (optimum pH). The reactor flasks were then equilibrated for 45 min at a constant temperature (20 ± 2°C).

Results and discussion

Effect of adsorbent modification on removal efficiency of CTX

The effect of adsorbent modification on the sorption capacity was evaluated at different experimental conditions. To investigate the CTX removal efficiency, standard activated carbon (SAC), ACP, and Fe@ACP adsorbents at varying pH levels were employed in the study. The results of this investigation are presented in Fig. 1a. Considering the performance of adsorbents at the pH range studied, the adsorbents showed removal efficiencies of CTX in the order of SAC < ACP < Fe@ACP. The CTX removal efficiency obtained using Fe@ACP (1.5 g ACP to 100 mL $FeCl_3$ (0.3 M)) was 85.7%. Fe@ACP exhibited the highest removal efficiency at a pH of 4.5, as observed in the results. This shows that the modification of adsorbent material improves their removal efficiency. Therefore, additional experiments were conducted using Fe@ACP to explore its adsorption capability at different operating conditions. In the first step, the optimization of ACP to $FeCl_3$ used to prepare Fe@ACP was done (ACP to ranging between 0.5 and 5 g in 100 mL $FeCl_3$ (0.3 M)). Then the synthesized adsorbents were used to remove CTX.

These experiments were conducted using a CTX solution at a concentration of 30 mg L^{-1} and a pH of 4.5. Fe@ACP prepared using different ratios of ACP to $FeCl_3$ was added at a dosage of 200 mg L^{-1} and equilibrated for 90 min. Figure 1b shows that ACP prepared without $FeCl_3$ induction, removed only 44.5% of the CTX. The CTX removal efficiency increased to 86.9% with the increase in the 2 g in 100 mL $FeCl_3$ (0.3 M)). With the further increase in the ACP to $FeCl_3$ the removal efficiency of CTX decreased. This shows that the modification of ACP by $FeCl_3$ at 2 g into 100 mL $FeCl_3$ results in an improvement of 42.4% in the removal efficiency compared to other concentration of ACP. These results show that the modification method employed in this study improves the effectiveness of the CTX removal. According to the obtained results, the continuation of the study was carried out using an ACP using $FeCl_3$ at 2 g in 100 mL $FeCl_3$.

Characterization of adsorbent

The FE-SEM micrographs in Fig. 2a,b were used to compare the surface morphology of ACP with that of Fe@ACP. As shown in Fig. 2a, the ACP exhibits a dense and relatively smooth surface. Figure 2b shows that the Fe@ACP also has a smooth surface but has cavities of various sizes scattered on the surface. This difference in the surface morphology between ACP and Fe@ACP is attributed to the activation procedure. This shows that adsorbent materials with high surface area can be prepared using low/no cost agricultural biomass materials using low-cost activation methods[38]. The pore sizes and pore volume were also shown to be higher in Fe@ACP compared to ACP. This is caused due to the high temperature of 800 °C used during the activation process. At this high temperature, the nitric acid that was impregnated on the adsorbent material is evaporated and released in the form of gas. Overall, the results obtained indicate that the activation method employed for the activated carbon has had a substantial impact on the structure and texture of the adsorbent, distinguishing it from the ACP.

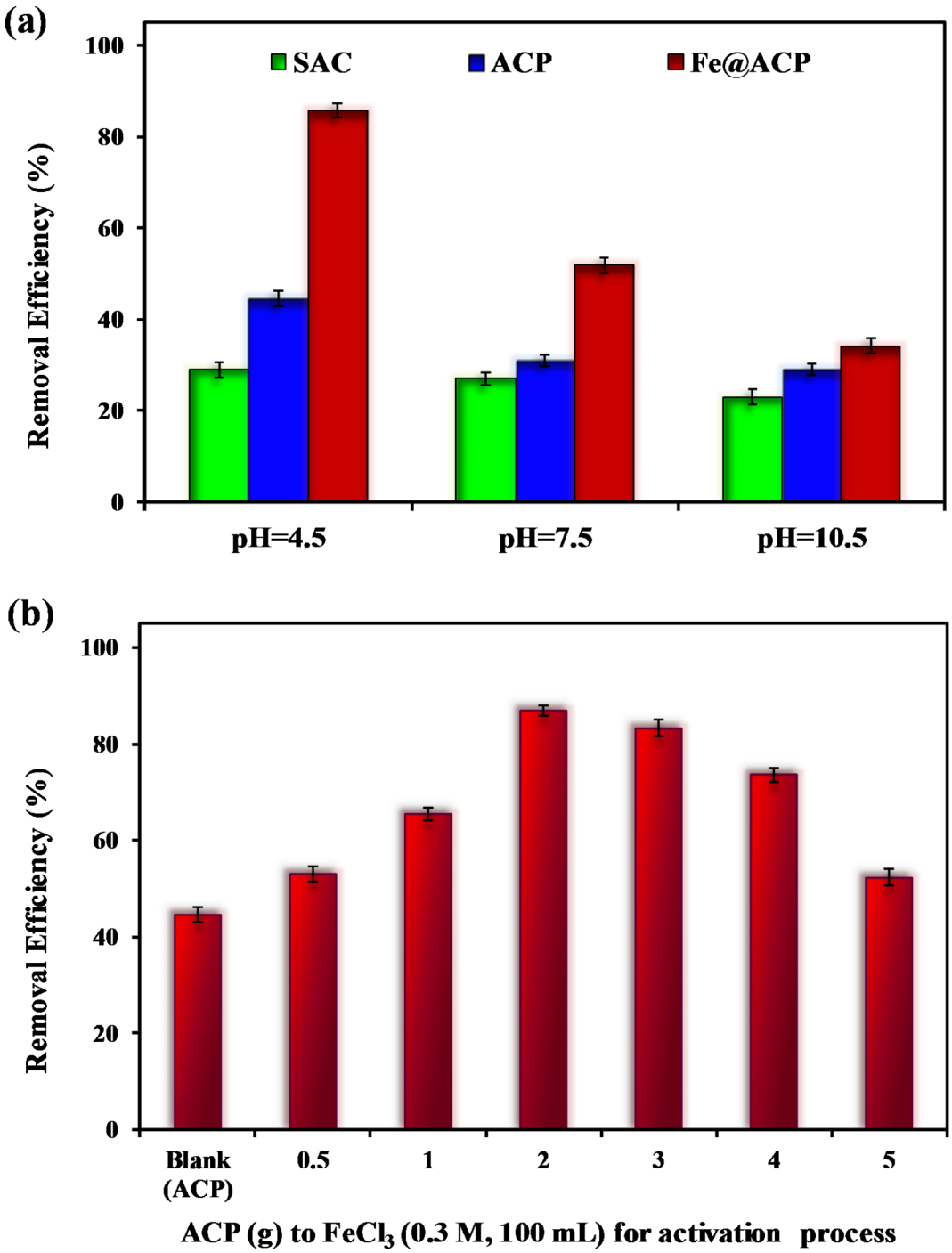

Fig. 1. (**a**) Removal efficiency of CTX at different pH obtained using SAC, ACP, and Fe@ACP, (**b**) Effect of $FeCl_3$ to ACP ratio in activation process, (operating condition: CTX concentration 30 mg L^{-1}, and adsorbent dose 200 mg L^{-1}, and reaction time of 90 min).

The pH_{pzc} of SAC, ACP, and Fe@ACP was found to be 7.3, 6.9, and 7.5 respectively, (see Fig. 2c). Understanding this behavior aids in the optimization of pH for effective adsorption process. At pH levels below pH_{pzc}, the surface of the adsorbent material exhibits a positive charge, while at pH levels higher than pH_{pzc}, it obtains a negative charge. Alam et al. used magnetic activated carbon from corn-cob biomass to remove acidic dyes, the pH_{pzc} in their study was obtained of 7.2[39].

Figure 2d and Table 2 present the surface area, average pore diameter, and pore structure characteristics of SAC, ACP, and Fe@ACP. Fe@ACP shows a high BET specific surface area of 1073 m^2 g^{-1}. This value higher than the surface area observed in ACP and SAC. The pore structure of the adsorbent material plays a crucial role in determining both the equilibrium capacity and the rate of removal during the adsorption process. As shown in Fig. 2d, the adsorption isotherm of N_2 obtained was fitted to the type IV curve according to the IUPAC

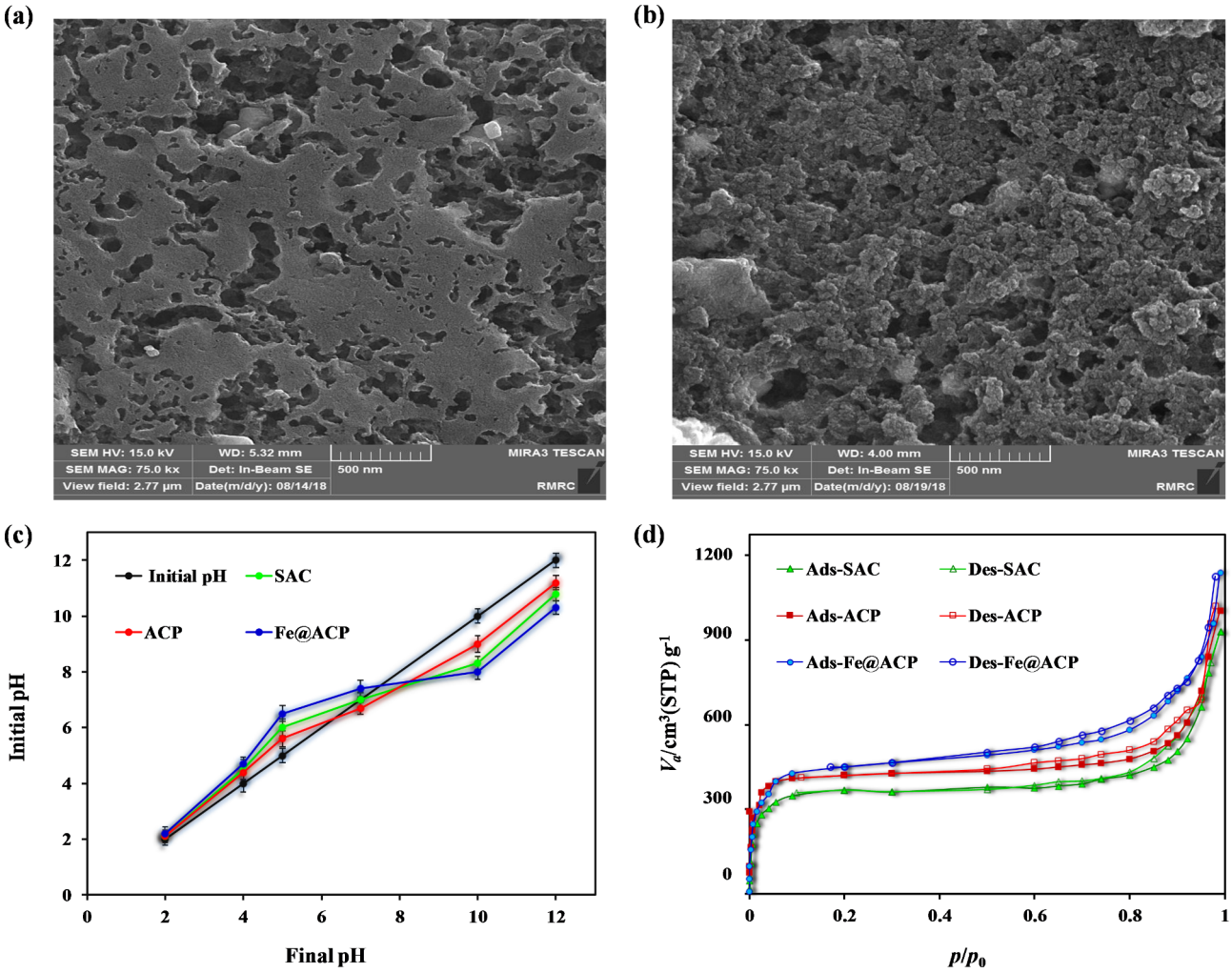

Fig. 2. FE-SEM images of (**a**) ACP and (**b**) Fe@ACP, (**c**) pH_{pzc} determination of Fe@ACP, (**d**) Nitrogen adsorption–desorption isotherm of SAC, ACP, and Fe@ACP.

Parameter	Unit	Value		
		SAC	ACP	Fe@ACP
Specific BET	$m^2\ g^{-1}$	914	987	1073
Total pore volume (P/P_0)	$cm^3\ g^{-1}$	0.67	0.86	0.88
Mean pore diameter	nm	6.3	5.7	5.1
Pore's structure	–	7.1	8.4	11.6
pH_{pzc}	–	7.3	6.9	7.5

Table 2. The main properties of the SAC, ACP, and Fe@ACP.

classification, with a closed hysteresis loop occurring at a P/P_0 value ranging from 0.45 to 0.98. This indicates that the samples contain numerous mesopores[40], the results that is consistent with the pore-size distributions. The pore sizes of all the three materials, SAC, ACP, and Fe@ACP, were in the range of 2–50 nm indicating they are mesoporous materials. In this isotherm at low concentration, the curve is steep indicating a monolayer adsorption. However, as depicted in Table 2, the specific BET surface areas and the total pore volume (P/P_0) were greatly increased for ACP and Fe@ACP due to modification, compared to SAC. ACP and Fe@ACP displayed higher surface characteristics than SAC, attributed to the combined thermal treatment and in-situ Fe modification. Safe et al. employed magnetic activated carbon as an adsorbent for the removal of imidacloprid. In this study, the adsorbent's BET surface area was calculated to be 1016 $m^2\ g^{-1}$, accompanied by an average pore volume of 0.69 $cm^3\ g^{-1}$, a micropore volume of 0.24 $cm^3\ g^{-1}$, and an average pore radius of approximately 1.81 nm[41]. In their study, *Zhou et al.* employed lignin-based magnetic carbon as a catalyst for peroxymonosulfate

activation to remove tetracycline. The synthesized magnetic carbon exhibited a total pore volume of 0.751 cm^3 g^{-1} and a specific surface area of 1122.9 m^2 g^{-1}[42].

The XRD pattern obtained for ACP and Fe@ACP are shown in Fig. 3a. At about 23.5°, broad peaks were observed which confirms the presence of active carbons with amorphous structure. Regarding Fe@ACP, the distinct peaks observed at 2θ values of 37.9° (3 1 1), 42.6° (4 0 0), 52.3° (4 2 2), and 58.1° (5 1 1) match to the characteristic peaks of the cubic phase Fe_3O_4, as identified by the JCPDS No. 19–0629[43].

Farahani et al. utilized magnetized activated carbon as a component in their research focused on ultrasonic-assisted magnetic dispersive solid-phase extraction. The XRD analysis performed in their study demonstrated

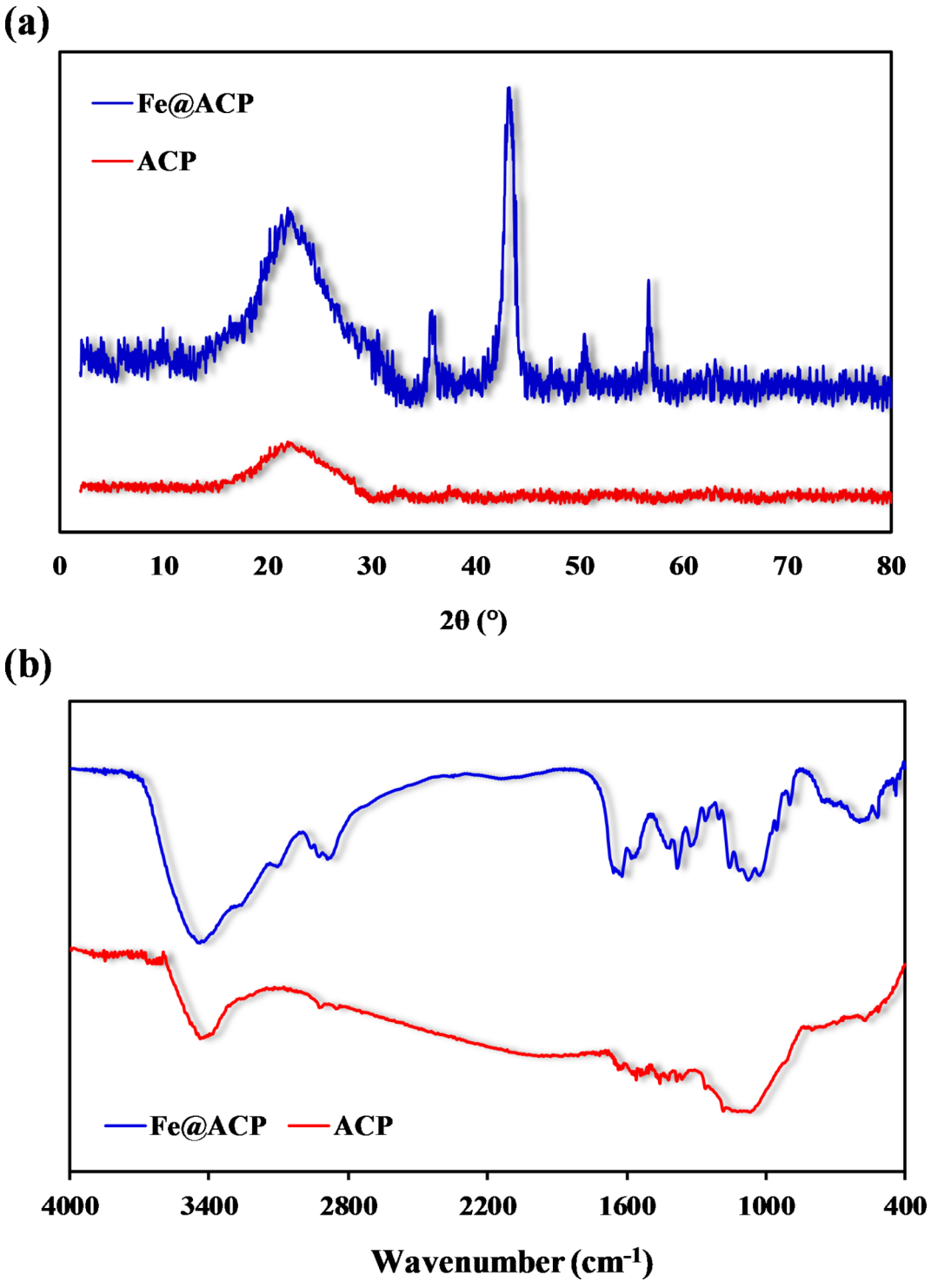

Fig. 3. (**a**) XRD patterns of Fe@ACP in the range of 2–80°, (**b**) FTIR spectra of ACP and Fe@ACP in the range of 4000–400 cm^{-1}.

that the positions and relative intensities of all diffraction peaks observed at 2θ values of 30.2°, 35.6°, 43.2°, 57.3°, and 62.9° match with the standard XRD data for the spinel structure Fe_3O_4. The lattice constants of α = 8.397 Å were found to align with the established reference (JCPDS 19–0629)[44]. Also, other studies observed the XRD pattern similar to the present study in the synthesis of magnetic active carbon and the formation of Fe_3O_4 (magnetite material)[45,46]. By utilizing the data obtained from the peak with the highest intensity (4 0 0), the average particle size was determined to be 11.6 nm.

The FTIR analysis allowed for the determination of the functional groups that exist on the surface of ACP and Fe@ACP. Figure 3b and Table 3 show the spectra obtained from the FTIR analysis of ACP and Fe@ACP. In the spectra of Fe@ACP, peaks at 612 cm^{-1}, 535 cm^{-1}, and 485 cm^{-1} appear which are otherwise absent for ACP. These peaks correspond to the Fe–O bond in the Fe@ACP created by the modification of ACP by $FeCl_3$[47]. This also indicated that Fe in the species form was attached to the surface of carbon. Furthermore, as seen, some identified peaks were shifted.

Development and evaluation of a regression model

The resulting matrix, along with the experimentally obtained response of CTX removal efficiency, is presented in Table 4.

ANOVA determines the adequacy of the resulting quadratic model and is shown in Table 5. *F*-value and *p*-value are determined as 52.48 and < 0.0001, respectively showing that the model is significant. The *p*-value is also less than 0.05, which indicates that the model terms X_1, X_2, X_3, X_4, and X_2^2 are significant.

The diagnostic plots in Fig. 4 confirm the model adequacy and predictability. The predictions derived from the proposed model exhibit favorable concurrence with the experimental results, as depicted in Fig. 4a. The internally studentized residuals obtained for the experimental response demonstrate a normal distribution, as illustrated in Fig. 4b. A linear profile without any large variations in the value of variance suggests a high degree of fitness for the predicted model. This finding validates the hypothesis that the error terms followed a normal distribution. The outlier plots for all the 30 experimental runs are shown in Fig. 4c. These plots depict the magnitude of the residual obtained for each experiment. A potential outlier is identified when its magnitude surpasses the general threshold of ±3% standard deviation (S.D.). Figure 4d illustrates that the internally studentized residuals exhibited a random distribution across all experimental runs, and their magnitudes remained within acceptable limits. Notably, the majority of the experimental data fell within the range of −2 to +2, indicating a confidence level of 95%. Consequently, no outliers were detected, confirming the accuracy of the model prediction. The residual versus predicted response plot is utilized to assess the independence of residuals with respect to the response value, with the expectation that they exhibit a random and dispersed pattern. If the plot exhibits a funnel shape, it can be inferred that the residual is linked to the mean value of the response variable.

This quadratic model is used to fit the correlation between the experimental variables and the outcome, which is the CTX removal efficiency. Through the utilization of Eq. (1) and fitting the experimental data presented in Table 4, a second order polynomial model was developed to describe the proposed model. The proposed model is expressed by Eq. (4) in the coded units as follow:

$$Y\,(\%) = 68.80 - 13.79X_1 - 5.74X_2 + 9.28X_3 + 5.38X_4 - 7.07X_2^2 \quad (4)$$

where X_1, X_2, X_3, and X_4 are the initial CTX concentration, pH of solution, adsorbent dosage, and reaction time, respectively. The intercept parameter (β_0 = 68.80%) denotes the average CTX removal efficiency when all the factors are fixed at their center point. The interaction of experimental conditions was found to not affect the removal efficiency of CTX. The developed model achieved an R^2 value of 0.9162, indicating that 91.62% of the total variations observed in the results could be attributed to the factors investigated in the study. The R^2 value was also very close to the adjusted R^2 (0.8987). The inclusion of variables in the model would lead to an increase in the R^2 value, while the adjusted R^2 value would decrease if the added variable is deemed insignificant. Hence, the close correspondence between the R^2 and adjusted R^2 values indicates that the model solely incorporates significant variables. In addition, the value of difference between the adjusted R^2 (0.8987) and predicted R^2

Wave number (cm^{-1})	Current work		Assignations
	ACP	Fe@ACP	
3430, 3433	3441	3453	Stretch of -OH
2922, 2883	2910 – 2851	2864, 2915	Stretch of C-H
1706, 1730	1704	1710	Stretch of C = O
1618, 1636	1612	1625	Stretch of C = O in carboxylic groups
1598, 1564	1575	1587	Stretch of C = C in aromatic rings
1420, 1402	1412	1408	Stretch of C-OH
1384, 1398	1392	1396	Symmetrical stretch of COO
1154, 1156	1138	1150	Asymmetrical stretch of C-O-C
1039, 1067	–	1064	Stretch of C-O
800 – 400	–	612, 535, 485	Stretch of Fe-O

Table 3. FTIR assignment of functional groups on ACP and the Fe@ACP.

Run	Actual values				Coded values				Removal efficiency (%)
	A (mg L^{-1})	B	C (mg L^{-1})	D (min)	X_1	X_2	X_3	X_4	
1	45	5	200	20	−1	−1	1	−1	90.0
2	45	9	100	20	−1	1	−1	−1	52.5
3	80	7	250	35	0	0	2	0	93.7
4	80	7	150	5	0	0	0	−2	52.2
5	80	7	150	65	0	0	0	2	85.0
6	80	7	150	35	0	0	0	0	68.8
7	80	7	150	35	0	0	0	0	67.1
8	115	5	100	50	1	−1	−1	1	56.2
9	45	9	100	50	−1	1	−1	1	63.8
10	80	7	50	35	0	0	−2	0	38.4
11	80	7	150	35	0	0	0	0	68.7
12	80	11	150	35	0	2	0	0	35.7
13	45	5	100	50	−1	−1	−1	1	80.6
14	45	9	200	50	−1	1	1	1	79.0
15	45	9	200	20	−1	1	1	−1	78.5
16	115	9	100	50	1	1	−1	1	40.3
17	115	5	200	50	1	−1	1	1	67.1
18	80	7	150	35	0	0	0	0	66.5
19	115	9	200	20	1	1	1	−1	40.0
20	10	7	150	35	−2	0	0	0	100.0
21	80	7	150	35	0	0	0	0	68.5
22	80	3	150	35	0	−2	0	0	42.0
23	115	9	200	50	1	1	1	1	51.9
24	80	7	150	35	0	0	0	0	67.5
25	115	9	100	20	1	1	−1	−1	31.8
26	45	5	100	20	−1	−1	−1	−1	76.2
27	115	5	200	20	1	−1	1	−1	56.7
28	150	7	150	35	2	0	0	0	48.0
29	115	5	100	20	1	−1	−1	−1	43.0
30	45	5	200	50	−1	−1	1	1	93.2

Table 4. Experimental design and results of CTX adsorption onto Fe@ACP.

Source	Sum of squares	Degree of freedom (df)	Mean squares	F-value	Probability *p*-value > F
Model	9557.6	5	1911.5	52.5	< 0.0001
X_1	4561.7	1	4561.7	125.2	< 0.0001
X_2	791.9	1	791.9	21.7	< 0.0001
X_3	2068.0	1	2068.0	56.8	< 0.0001
X_4	694.7	1	694.7	19.1	0.0002
X_2^2	1441.4	1	1441.4	39.6	< 0.0001
Residual	874.1	24	36.4	-	-
Lack of fit	822.2	19	43.3	4.2	0.0603
Pure error	51.9	5	10.4	–	–
Cor total	10431.8	29	–	–	–

Table 5. ANOVA for model development of CTX adsorption onto Fe@ACP.

(0.8217) is < 0.2, confirming a good fit of the model. On the other hand, the p- and *F*-values of 0.0603 and 4.17, respectively obtained for model lack-of-fit, were found to be statistically insignificant and negligible compared to pure error. This further supports the suitability of the proposed model. The perturbation plot in Fig. 5a illustrates the relative impacts of each experimental variable on the removal efficiency of CTX, allowing for a comparative analysis.

The perturbation plot in Fig. 5a illustrates the relative impacts of each experimental variable on the removal efficiency of CTX, allowing for a comparative analysis. The initial concentration of CTX, adsorbent dosage, and

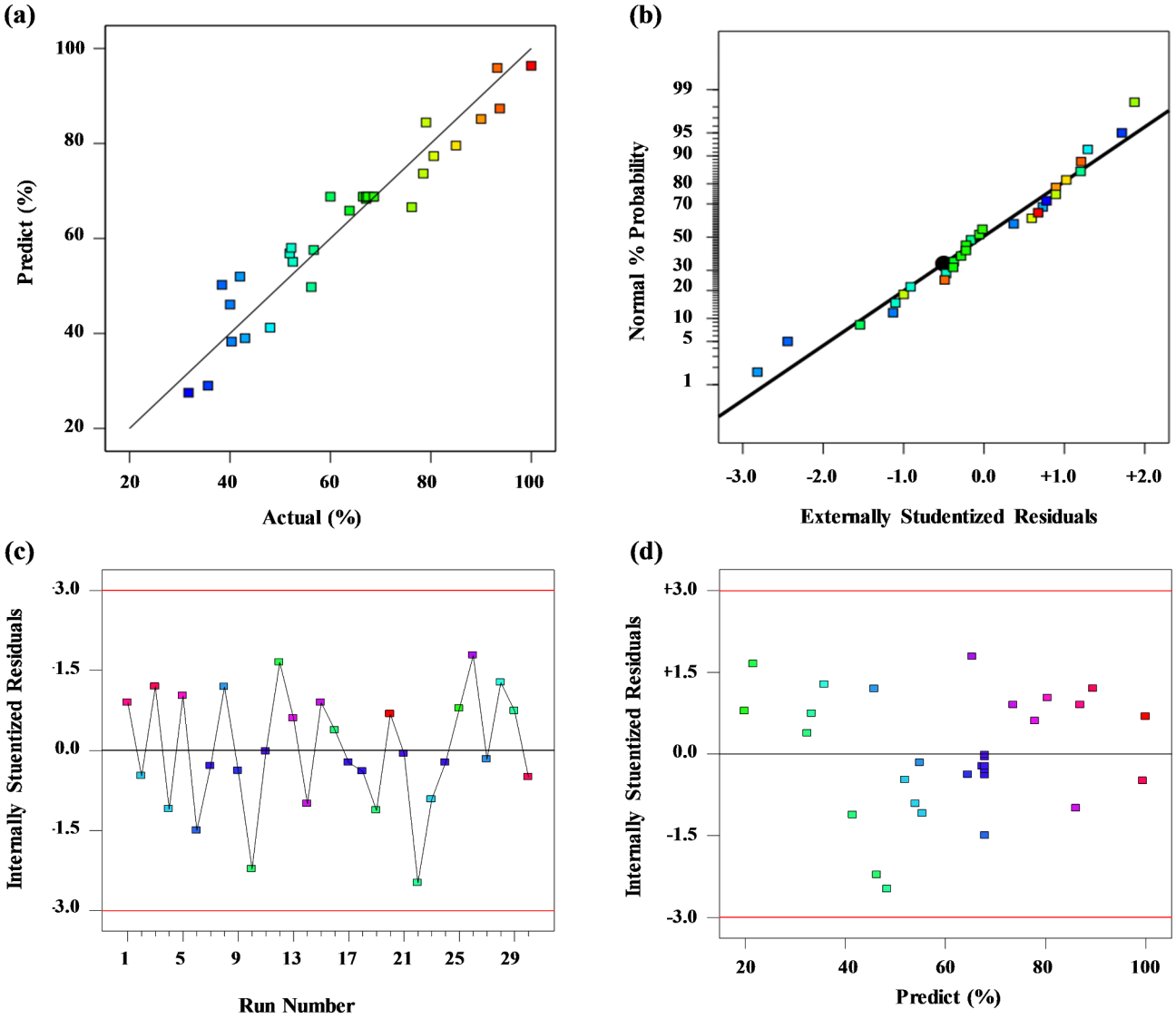

Fig. 4. (**a**) Predicted versus actual values. (**b**) Normal % probability versus internally studentized residuals plot. (**c**) Internally studentized residuals versus run plot. (**d**) Internally studentized residuals versus predicted plot.

reaction time showed diagonal lines, showing that they are effective variables in the adsorption of CTX on Fe@ACP. The pH curve shows a steep curvature, representing that the response of removal efficiency of CTX by adsorption on Fe@ACP was very sensitive to this variable.

The effect of initial concentration of CTX and pH of solution on the removal efficiency of CTX using Fe@ACP at a dosage of 150 g L^{-1} and the equilibration time of 35 min is shown in Fig. 5b as a 3D plot. As the concentration of CTX was raised from 10 to 150 mg L^{-1}, there was a corresponding decrease in the removal efficiency of CTX, dropping from 96.7 to 41.6%. This observation indicates that the removal efficiency at high CTX concentrations is significantly influenced by the CTX concentration. This phenomenon can be ascribed to the saturation of adsorption sites on the surface of the adsorbent material. On the other hand, at higher concentrations of CTX, the loading capacity of the adsorbent also increases due to the increase in driving force for mass transfer of CTX onto the adsorbent surface[17].

The pH of the solution affects both the adsorbent and the adsorbate. The net surface charge of Fe@ACP is a function of solution pH. Fe@ACP shows a net positive charge at solution pH below 7.2 and a negative charge at pH above 7.2. On the other hand, CTX has two pKa values of 3.4 and 6.7. This indicates that it is ionized due to the changes in the pH of the solution. At a solution pH < 3.4, CTX is positively charged as amine groups become protonated. In between 3.4 and 6.7, the surface charges are neutralized. At pH > 6.7, the carboxylic group loses its proton and obtains two negative charges. The pH of the solution was systematically changed across a range of 3 to 11 during the conducted experiments. This led to a decrease of only 23% in the CTX removal efficiency using Fe@ACP. The impact of pH on the removal efficiency of CTX was comparatively insignificant in relation to the effects observed with the initial CTX concentration and adsorbent dosage.

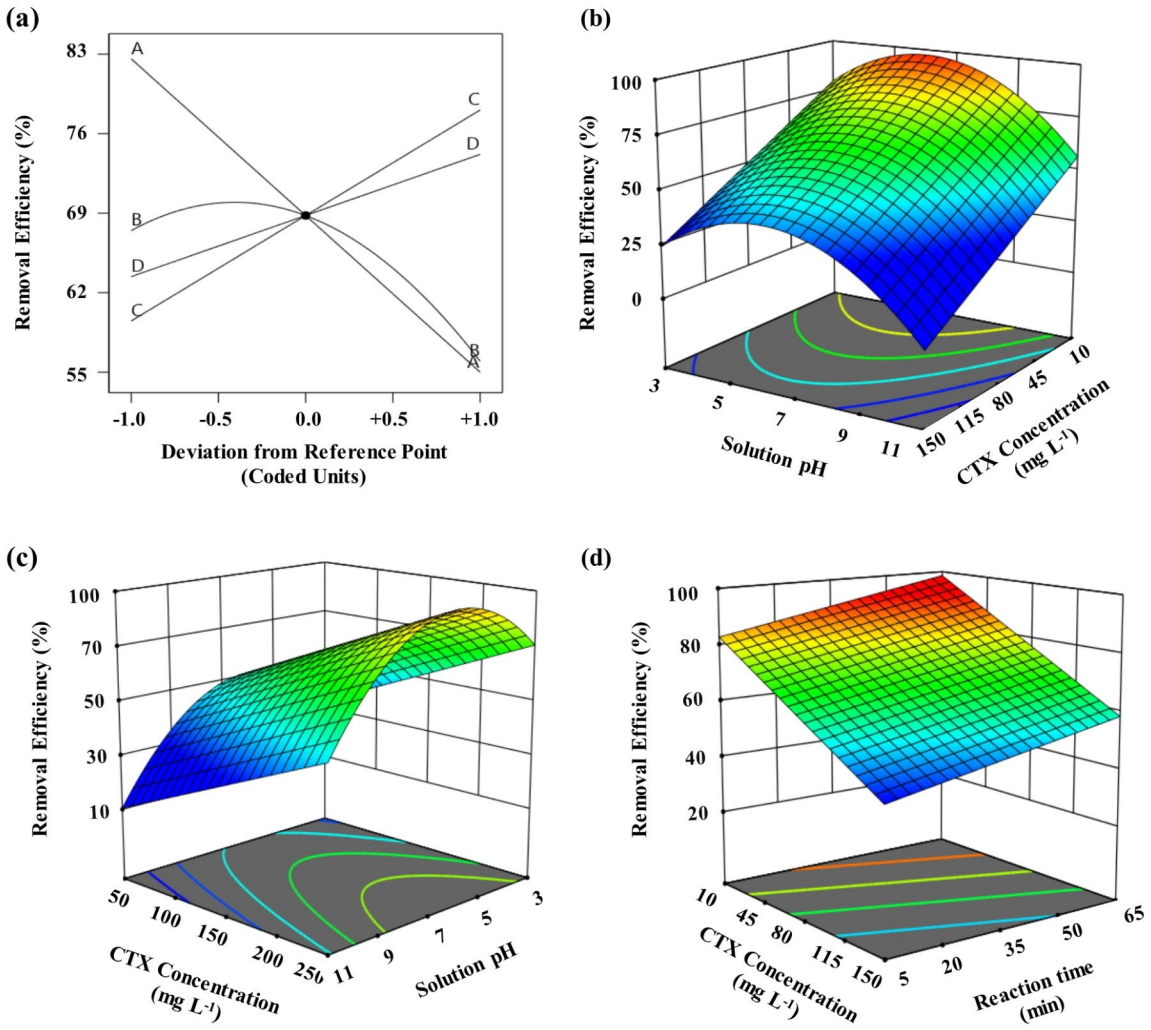

Fig. 5. (**a**) perturbation plot, (**b**) Effect of initial concentration of CTX and pH, (**c**) Effect of adsorbent dose and pH, (**d**) Effect of initial concentration of CTX and equilibration time, (operating parameters set at their central points including: Initial concentration of CTX of 80 mg L^{-1}, adsorbent dose of 150 mg L^{-1}, pH of 7.0, and reaction time of 35 min).

From Fig. 5b, it is also evident that the pH of the solution shows a quadratic effect on the CTX removal efficiency. A maximum removal efficiency of 77.5% is observed at neutral pH of about 6.7–7.2. The pH_{pzc} of the adsorbent and pK_a of the adsorbate, shows that a minimum CTX removal efficiency occurs when CTX was ionized at acidic pH (less than 3.4) or alkaline pH (higher than 7.2). The maximum removal is observed when CTX is negatively charged and Fe@ACP is positively charged over the solution pH range of 6.7–7.2. At a pH greater than 7.2, both adsorbent and adsorbate are negatively charged, leading to repulsive electrostatic forces between them.

The effect of adsorbent dosage and pH on the CTX removal efficiency using Fe@ACP is depicted in Fig. 5c. The dosage of the adsorbent has a substantial impact on the efficiency of adsorption. The CTX removal efficiency exhibited an upward trend, rising from 47.5 to 87.6%, as the adsorbent dosage was increased from 50 to 250 g L^{-1}. This is due to the increase in the number of adsorption sites at higher dosages. Conversely, the equilibrium adsorption capacity of Fe@ACP demonstrates a consistent decline as the adsorbent dosage increases. This is due to the decrease in the amount of accessible CTX molecules in the aqueous phase per sorption site and increase in the number of unsaturated sorption sites[18].

The effect of equilibration time and initial CTX concentration on the removal efficiency of CTX is shown in Fig. 5d. Contrary to the other experimental variables in the adsorption process, the equilibration time does not vary significantly at different process conditions. In most scenarios, the adsorption is rapid for the first few minutes of contact and then proceeds at a slower pace until equilibrium is reached. The equilibration time was

varied from 5 to 65 min and the results show that CTX removal occurs in a two-stage process, an initial rapid adsorption followed by slow paced adsorption.

Most of the CTX molecules were adsorbed during the initial 45 min and the removal efficiency leveled off after 45 min. The initial rapid adsorption can be attributed to the diffusion process, wherein CTX molecules move from the solution towards the external surface of Fe@ACP. Then, the CTX molecules are transported to the inner pores of the Fe@ACP. This is followed by a slow diffusion to the adsorption site. The experimental results show that after 45 min of shaking, a steady equilibrium state was achieved[17].

Pareto analysis was also employed to elucidate the contribution of significant variables within the model. The percentage effect (P_e) of each factor on the response, which is the CTX removal efficiency, was determined using the following equation:

$$P_e = \frac{c_i^2}{\sum c_i^2} \times 100 \quad (i \neq 0) \tag{5}$$

In the equation, P_e represents the percentage effect of the i^{th} term in the model, while C_i denotes the coefficient of the i^{th} parameter in the model. Based on the above analysis, initial concentration of CTX (49.0%), pH of solution (8.5%), adsorbent dosage (22.2%), equilibration time (7.5%), and quadratic effect of solution pH (12.9%) are the significant effective parameters of the model, respectively (see Fig. 6).

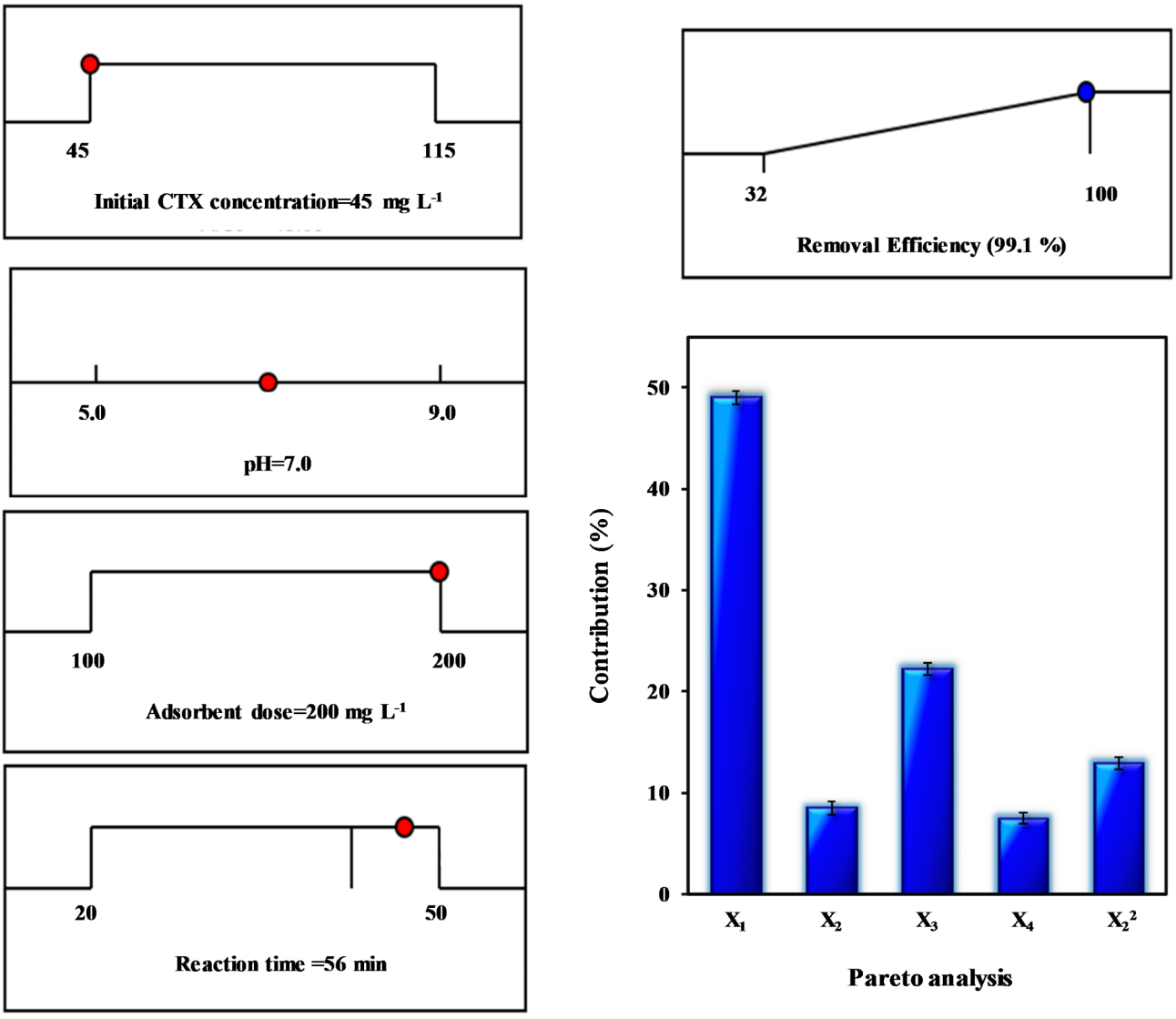

Fig. 6. Desirability ramp for numerical optimization of CTX removal, and contribution (%) of parameters on the CTX removal (Pareto analysis).

Initial CTX concentration (mg L^{-1})	pH	Adsorbent dose (mg L^{-1})	Reaction time (min)	Predicted removal efficiency (%)	95% PI low	95% PI high	Experimental removal efficiency (%)
45	7	200	56	99.4	94	100	99.1
80	6.5	100	60	70.1	64	75	69.7
115	6.2	200	60	74.5	68	81	73.9
45	6.0	200	20	88.0	82	930	87.8

Table 6. Validation of the CTX removal efficiency model.

Isotherms						
Isotherms	**Non-linear equation**	**Constants**	X^2	**SSE**	**Adj. R^2**	**AIC**
Langmuir	$q_e = \frac{q_m b C_e}{1+bC_e}$	b = 1.71 L mg^{-1} q_m = 651.6 mg g^{-1}	0.097	0.153	0.9931	0.62
Freundlich	$q_e = k_F C_e^{\frac{1}{n}}$	K_f = 27.4 (mg g^{-1}) (mg^{-1})$^{1/n}$ n = 6.2	0.091	0.651	0.9902	1.12
Sips	$q_e = \frac{K_s C_e^{\beta S}}{1+m_S C_e^{\beta S}}$	q_m = 572 mg g^{-1} K_S = 0.94 (L mg^{-1})^{ms} m_s = 0.517	0.084	0.923	0.9614	10.4
Kinetics						
Kinetics	**Nonlinear form**	**Constants**	χ^2	**SSE**	**Adj. R^2**	**AIC**
First-order	$q_t = q_e(1 - e^{-K_1 t})$	q_e = 371.7 mg g^{-1} k = 0.216 min^{-1}	0.086	0.509	0.9810	1.93
Second-order	$q_t = \frac{K_2 q_e^2 t}{1+q_e t K_2}$	q_e = 401.8 mg g^{-1} k = 0.103 g mg^{-1} min^{-1}	0.044	0.418	0.9934	0.66
Intra-particle diffusion	$q_t = K_{id}\sqrt{t} + C$	k_{id} = 0.848 mg (g $min^{1/2}$)$^{-1}$ C = 0.319 mg g^{-1}	0.106	0.613	0.9714	2.81

Table 7. The non-linear parameters of kinetics and isotherms models for adsorption of CTX onto Fe@ACP.

Process optimization and validation

In the numerical optimization procedure of Design-Expert software, the expected goals for all the experimental variables and response were set from the menu. A successfully optimized model will result in finding the process conditions for designing a CTX removal unit working with highest efficiency and desirability. In addition, the response for specific set of operating conditions can be determined. In this study, the goal was to maximize the removal efficiency of CTX as presented in Fig. 6. When the experimental variables are set at their optimum level, the maximum removal efficiency of CTX is obtained.

Further experiments were conducted to validate the model by using a set of random operating conditions. The obtained removal efficiency was compared to the predicted response of the model. The results of the validation experiment runs and the predicted responses from the model are compared in Table 6. The validation experiments efficiency results that are within a 95% range of the predicted values, thus demonstrating the appropriateness and suitability of the developed regression model[19].

Adsorption kinetics and isotherms

Table 7 presents the kinetic and isotherm parameters obtained for the CTX adsorption on Fe@ACP. The second order model demonstrates a higher R^2 value and is better suited for describing the adsorption phenomenon in comparison to the first order and intra-particle diffusion models. The second order kinetics in the absorption process of CTX onto Fe@ACP indicates possible chemical absorption. According to Weber and Morris, if the rate limiting step is the intraparticle diffusion, then the adsorbed amount at any time t should be directly proportional to the square root of contact time t and should pass through the origin. However, according to obtained results, the intraparticle diffusion model has effect on the adsorption process but is not limiting step because the values do not tend to the origin[48]. The adsorption equilibrium isotherm was well-fitted using the Langmuir isotherm equation in comparison to the Freundlich equation. Langmuir isotherm indicates that the adsorption of CTX onto Fe@ACP was a monolayer surface adsorption without interaction between adsorbed molecules. The value of n was more than 1, confirming that the CTX adsorption onto Fe@ACP was preferential. The obtained values of R_L ranging 0–1 also imply that the adsorption process was favorable.

Adsorbent reusability and regenerating

Reusability is also an important factor of an adsorbent. From an economic perspective, it is essential to synthesis stable adsorbents that can be regenerated under realistic conditions for multiple reuses. The experiments were carried out using 500 mg of CTX-loaded into adsorbent for 24 h at 100 rpm in the optimum condition. Then, the separated adsorbents were dried and used for desorption experiments. to conduct the desorption process, the

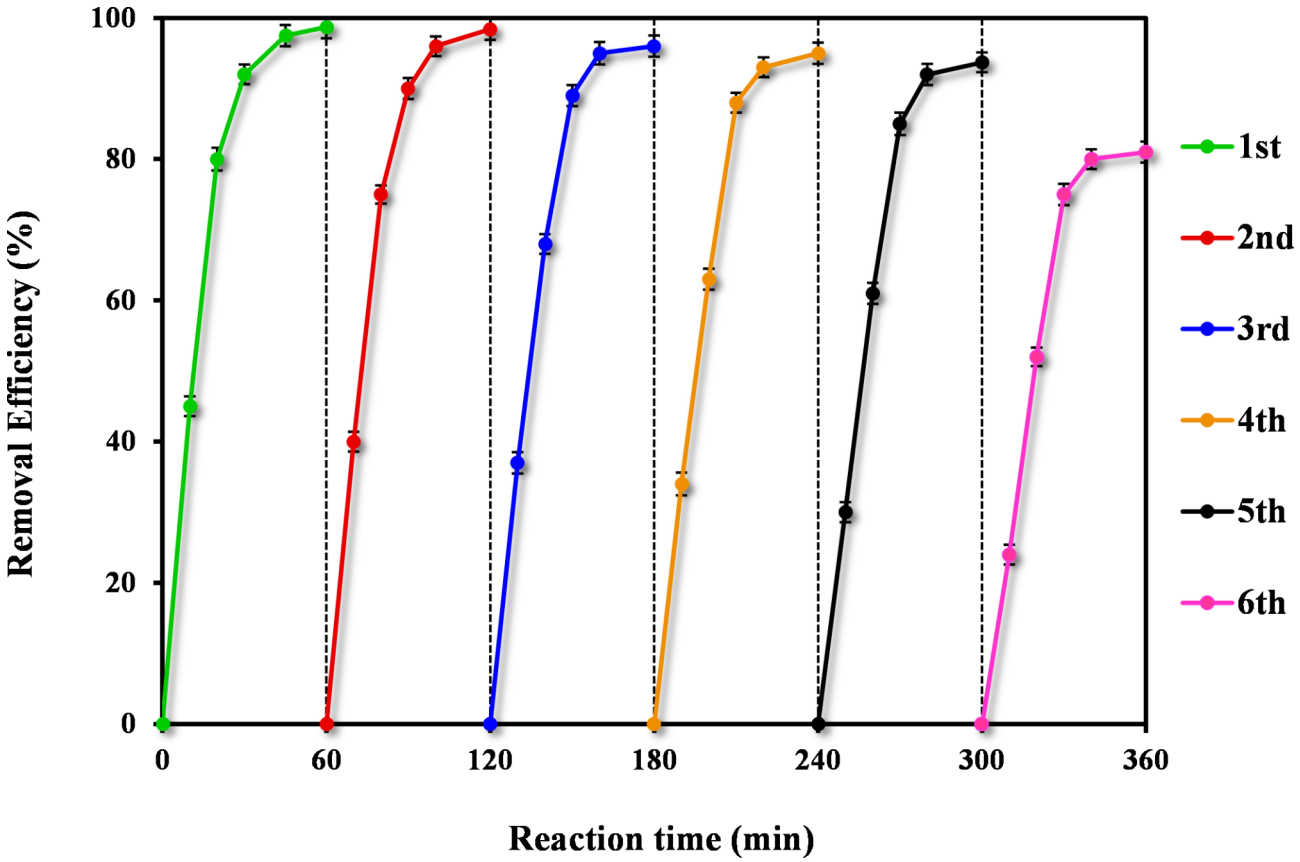

Fig. 7. Regeneration performance of Fe@ACP using NaOH in the CTX removal efficiency throughout 6 cycle (operating condition: CTX concentration of 45 mg L^{-1}, solution pH of 7, and adsorbent of 200 mg L^{-1}).

AC source	Modifier	Pollutant	q_m (mg g^{-1})	S_{BET} (m^2 g^{-1})	Removal (%)	Ref
Pomegranate wood	NH_4Cl	Amoxicillin	437	1029	> 99.0	29
Almond green hull	Magnetic AC coated with CuS	Tetracycline	13.514	186.83	70.0	50
Commercial activated carbon	Magnetic activated carbon/chitosan	Ciprofloxacin	90.10	204	82.0	51
		Erythromycin	178.57		54.0	
		Amoxicillin	526.31		72.0	
Bagasse	Magnetic biochars	Sulfamethoxazole	419.8	386.3	100	52
Charcoal type lignite- based	$FeCl_3$	Organic micropollutants	111.1	984	> 75%	53
Charcoal type coconut-based	$FeCl_3$		58.8	1187	> 85%	
Pistachio shell	$FeCl_3$	Cefotaxime	651.6	1073	99.1	Current study

Table 8. Comparison of characteristic properties of Fe@ACP with some other modified activated carbon as adsorbent.

saturated adsorbent was added into 200 mL of NaOH 0.2 M. After 24 h contact time, the regenerated adsorbent particles were separated and dried. The obtained results revealed the breakthrough curves of CTX removal efficiency within 6 cycles in the optimum condition. It can be seen that the CTX removal efficiency just slightly reduces with the increase of regeneration times, and is still in high level (93.8%) after 5 cycles of regeneration, which accounts for 94.6% of its initial adsorption capacity (see Fig. 7). After the 6th cycle, the CTX removal efficiency decreases significantly (81.4%). It indicates that Fe@ACP is a high-performance adsorbent with a good reusability for adsorption and desorption of CTX after 5 cycles of regeneration.

The comparison of the employed adsorbent (Fe@ACP) characteristics with the other employed modified activated carbon with various agents summarized in Table 8. Although the process requires further optimization and upscaling, the Fe@ACP has demonstrated its potential as a superior alternative to existing commercial ACs due to its ability to be regenerated and reused, and its possibility for magnetic harvesting, which obviates the need to invest in large flocculation and sedimentation tanks.

Hospital wastewater treatment

Wastewater samples were collected from a hospital and subsequently stored at a temperature of 4 °C before undergoing analysis. All measurements were conducted in triplicates. Following that, the samples were subjected to filtration using filter paper possessing a pore size of 0.45 µm. The resulting filtrate, obtained from a 200 mL aliquot, was concentrated to a volume of 10 mL using a rotary evaporator equipped with a vacuum pump V-700. The evaporation process was performed under reduced pressure conditions while maintaining a constant temperature of 50 °C. To clean up the samples, a Visiprep® solid-phase extraction system equipped with a mini vacuum pump (USA) was utilized. Oasis® HLB cartridges (60 mg, 3 mL^{-1}) manufactured by Waters (USA) and C_{18} cartridges (50 mg, 1 mL^{-1}) by Supelco (USA) were employed for the process. The cartridges underwent conditioning with a solution comprising 10 mL of a 1:1 mixture of methanol and water. Subsequently, a 10 mL portion of the sample, which had been pre-concentrated through evaporation, was sequentially passed through C_{18} and HLB cartridges at a flow rate of 1.0 mL min^{-1}. Subsequently, the cartridge was rinsed with 5 mL of deionized water, allowed to air dry, and the target analytes were extracted using 10 mL of acetone from the Oasis HLB cartridge, and 10 mL of a solution containing methanol and aqueous formic acid (0.05%) in a 55:45 ratio from the C_{18} cartridge. The eluents from both cartridges were consolidated and subjected to evaporation under a nitrogen stream until the volume reached 2.0 mL[49]. A portion of the sample was analyzed using the HPLC method proposed in this study. Based on the results obtained, it was observed that the concentration of CTX in the hospital wastewater samples decreased from 14.06 ± 0.57 µg L^{-1} to zero following the implementation of the adsorption process under optimal conditions.

Conclusion

To optimize the critical adsorption parameters including the initial CTX concentration, pH, adsorbent dosage, and reaction time, the RSM employing CCD was implemented. The CTX maximum removal efficiency of 99.1% found. The non-linear second order kinetic model exhibited a favorable fit to the experimental data, while the Langmuir isotherm model demonstrated its capability to accurately describe the equilibrium results obtained. Adsorption non-linear kinetics and isotherms confirmed the occurrence of monolayer adsorption through chemisorption mechanism. The results obtained from the analysis of real samples indicated that the initial CTX concentration in hospital wastewater, measured at 14.06 ± 0.57 µg L^{-1}, was effectively reduced to zero after implementing the optimal conditions of the proposed treatment process. Accordingly, the mesoporous adsorbent Fe@ACP is introduced as a promising solution for water pollution management due to its notable characteristics, such as high pore volume and specific surface area, derived from an economically viable agricultural biomass source. This approach not only offers significant environmental benefits but also represents a valuable and cost-effective strategy in addressing water pollution challenges.

Data availability

The dataset used and/or analyzed during the current study are available from the corresponding author on reasonable request.

Received: 10 July 2024; Accepted: 11 October 2024
Published online: 02 December 2024

References

1. Li, N., Zhou, L., Jin, X., Owens, G. & Chen, Z. Simultaneous removal of tetracycline and oxytetracycline antibiotics from wastewater using a ZIF-8 metal organic-framework. *J. Hazard. Mater.* **366**, 563–572 (2019).
2. Kumar, J. A. et al. Enhanced PAHs removal using pyrolysis-assisted potassium hydroxide induced palm shell activated carbon: batch and column investigation. *J. Mol. Liq.* **279**, 77–87 (2019).
3. Namasivayam, S. K. R. et al. Aquatic biomass cellulose fabrication into cellulose nanocomposite and its application in water purification. *J. Clean. Prod.* **396**, 136386 (2023).
4. Anish, M. et al. An evaluation of biosynthesized nanoparticles in biodiesel as an enhancement of a VCR diesel engine. *Fuel.* **328**, 125299 (2022).
5. Fayaz, T., Renuka, N. & Ratha, S. K. Antibiotic occurrence, environmental risks, and their removal from aquatic environments using microalgae: advances and future perspectives. *Chemosphere.* **349**, 140822 (2024).
6. Badawi, A. K. et al. Advancing cobalt ferrite-supported activated carbon from orange peels for real pulp and paper mill wastewater treatment. *Desalination Water Treat.* **318**, 100331 (2024).
7. Santos, F., Almeida, C. M. R., Ribeiro, I. & Mucha, A. P. Potential of constructed wetland for the removal of antibiotics and antibiotic resistant bacteria from livestock wastewater. *Ecol. Eng.* **129**, 45–53 (2019).
8. Fu, T. et al. Synthesis and application of wetland plant-based functional materials for aqueous antibiotics removal. *Sci. Total Environ.* **908**, 168214 (2024).
9. Jang, H. M., Choi, S., Shin, J., Kan, E. & Kim, Y. M. Additional reduction of antibiotic resistance genes and human bacterial pathogens via thermophilic aerobic digestion of anaerobically digested sludge. *Bioresour. Technol.* **273**, 259–268 (2019).
10. Yuju, S., Xiujuan, T., Dongsheng, S., Zhiruo, Z. & Meizhen, W. A review of tungsten trioxide (WO3)-based materials for antibiotics removal via photocatalysis. *Ecotoxicol. Environ. Saf.* **259**, 114988 (2023).
11. Deivasigamani, P. et al. Deep insights into kinetics, optimization and thermodynamic estimates of methylene blue adsorption from aqueous solution onto coffee husk (coffee arabica) activated carbon. *Environ. Res.* **236**, 116735 (2023).
12. Tran, D-T., Ha, T-H., Vu, T-P-T., Nguyen, V-N. & Pham, T-D. Novel CeO2-V2O5/rGO tertiary photocatalyst for improved cefotaxime degradation using visible-light. *Inorg. Chem. Commun.* **161**, 112044 (2024).
13. León, D. E., Zúñiga-Benítez, H., Peñuela, G. A. & Mansilla, H. D. Photocatalytic removal of the antibiotic cefotaxime on TiO 2 and ZnO suspensions under simulated sunlight radiation. *Water Air Soil Pollut.* **228**, 1–12 (2017).
14. Ribeiro, A. R., Sures, B. & Schmidt, T. C. Cephalosporin antibiotics in the aquatic environment: a critical review of occurrence, fate, ecotoxicity and removal technologies. *Environ. Pollut.* **241**, 1153–1166 (2018).
15. Lei, J., Duan, P., Liu, W., Sun, Z. & Hu, X. Degradation of aqueous cefotaxime in electro-oxidation—electro-Fenton—persulfate system with Ti/CNT/SnO2–Sb–Er anode and Ni@ NCNT cathode. *Chemosphere.* **250**, 126163 (2020).

16. Ben, Y. et al. Human health risk assessment of antibiotic resistance associated with antibiotic residues in the environment: a review. *Environ. Res.* **169**, 483–493 (2019).
17. Hamadeen, H. M. & Elkhatib, E. A. New nanostructured activated biochar for effective removal of antibiotic ciprofloxacin from wastewater: Adsorption dynamics and mechanisms. *Environ. Res.* **210**, 112929 (2022).
18. Saeed-Ul-Hassan, M. et al. A comparative study of moisture adsorption on GO, MOF-5, and GO/MOF-5 composite for applications in atmospheric water harvesting. *Nanoscale Adv.* (2024).
19. Zheng, S. et al. Current progress in natural degradation and enhanced removal techniques of antibiotics in the environment: a review. *Int. J. Environ. Res. Public Health*. **19** (17), 10919 (2022).
20. Wang, X., Jing, J., Zhou, M. & Dewil, R. Recent advances in H2O2-based advanced oxidation processes for removal of antibiotics from wastewater. *Chin. Chem. Lett.* **34** (3), 107621 (2023).
21. Zhang, Y., Zhao, Y-G., Maqbool, F. & Hu, Y. Removal of antibiotics pollutants in wastewater by UV-based advanced oxidation processes: influence of water matrix components, processes optimization and application: a review. *J. Water Process. Eng.* **45**, 102496 (2022).
22. Dai, C. et al. Construction of a novel integrated electrochemical oxidation-coagulation system for simultaneous removal of suspended solids and antibiotics. *Chem. Eng. J.* **447**, 137505 (2022).
23. Al Alwan, B., Ismail, B., El Jery, A. & Badawi, A. K. State-of-the-art strategies for microplastics mitigation in aquatic environments: identification, technological innovations, and prospects for advancement. *J. Water Process. Eng.* **61**, 105336 (2024).
24. Badawi, A. K., Kriaa, K., Osman, R. M. & Hassan, R. Modified Rice Husk Waste-based filter for Wastewater Treatment: pilot study and reuse potential. *Chem. Eng. Technol.* **47** (7), 968–975 (2024).
25. Ehtisham, M., Badawi, A. K., Khan, A. M., Khan, R. A. & Ismail, B. Exploring moisture adsorption on cobalt-doped ZnFe 2 O 4 for applications in atmospheric water harvesting. *RSC Adv.* **14** (9), 6165–6177 (2024).
26. Hassan, R., Alluqmani, A. E. & Badawi, A. K. An eco-friendly solution for greywater treatment via date palm fiber filter. *Desalination Water Treat.* **317**, 100163 (2024).
27. Elawwad, A., Karam, A. & Zaher, K. Using an algal photo-bioreactor as a polishing step for secondary treated wastewater. *Pol. J. Environ. Stud.* ;**26**(4). (2017).
28. Gangupomu, R. H., Sattler, M. L. & Ramirez, D. Comparative study of carbon nanotubes and granular activated carbon: physicochemical properties and adsorption capacities. *J. Hazard. Mater.* **302**, 362–374 (2016).
29. Moussavi, G., Alahabadi, A., Yaghmaeian, K. & Eskandari, M. Preparation, characterization and adsorption potential of the NH4Cl-induced activated carbon for the removal of Amoxicillin antibiotic from water. *Chem. Eng. J.* **217**, 119–128 (2013).
30. Saleh, T. A., Adio, S. O., Asif, M. & Dafalla, H. Statistical analysis of phenols adsorption on diethylenetriamine-modified activated carbon. *J. Clean. Prod.* **182**, 960–968 (2018).
31. Shaarani, F. W. & Hameed, B. H. Ammonia-modified activated carbon for the adsorption of 2,4-dichlorophenol. *Chem. Eng. J.* **169** (1), 180–185 (2011).
32. Goswami, M. & Phukan, P. Enhanced adsorption of cationic dyes using sulfonic acid modified activated carbon. *J. Environ. Chem. Eng.* **5** (4), 3508–3517 (2017).
33. Yang, N., Zhu, S., Zhang, D. & Xu, S. Synthesis and properties of magnetic Fe3O4-activated carbon nanocomposite particles for dye removal. *Mater. Lett.* **62** (4–5), 645–647 (2008).
34. Bhan, M., Satija, S., Garg, C., Dureja, H. & Garg, M. Optimization of ionic liquid-based microwave assisted extraction of a diterpenoid lactone-andrographolide from Andrographis paniculata by response surface methodology. *J. Mol. Liq.* **229**, 161–166 (2017).
35. Jang, J. & Lee, D. S. Magnetite nanoparticles supported on organically modified montmorillonite for adsorptive removal of iodide from aqueous solution: optimization using response surface methodology. *Sci. Total Environ.* **615**, 549–557 (2018).
36. Najafpoor, A. et al. Optimization of anionic dye adsorption onto Melia azedarach sawdust in aqueous solutions: effect of calcium cations. *Asia-Pac. J. Chem. Eng.* **11** (2), 258–270 (2016).
37. Tran, H. N., You, S-J., Hosseini-Bandegharaei, A. & Chao, H-P. Mistakes and inconsistencies regarding adsorption of contaminants from aqueous solutions: a critical review. *Water Res.* **120**, 88–116 (2017).
38. Zhang, D., Huo, P. & Liu, W. Behavior of phenol adsorption on thermal modified activated carbon. *Chin. J. Chem. Eng.* **24** (4), 446–452 (2016).
39. Alam, S. et al. Fabrication of magnetic activated carbon from corn-cob biomass for the removal of acidic dyes from wastewater. *Desalination Water Treat.* **317**, 100049 (2024).
40. Yusop, M. F. M., Abdullah, A. Z. & Ahmad, M. A. Amoxicillin adsorption from aqueous solution by Cu (II) modified lemon peel based activated carbon: mass transfer simulation, surface area prediction and F-test on isotherm and kinetic models. *Powder Technol.* **438**, 119589 (2024).
41. Safe, Y. L., Springer, V. & Avena, M. A sustainable and fast methodology based on magnetic activated carbon for removal of imidacloprid from aqueous solution. *J. Environ. Chem. Eng.* **11** (5), 111135 (2023).
42. Zhou, H. et al. Insights into novel lignin-based magnetic carbon enabling peroxymonosulfate activation for tetracycline removal: performance, mechanism and application. *Sep. Purif. Technol.* **332**, 125961 (2024).
43. Jonidi Jafari, A. et al. Fenton-like catalytic oxidation of tetracycline by AC@Fe3O4 as a heterogeneous persulfate activator: adsorption and degradation studies. *J. Ind. Eng. Chem.* **45**, 323–333 (2017).
44. Farahani, H. S., Najafi, M., Behbahani, M. & Naseri, M. T. Ultrasonic assisted magnetic dispersive solid phase extraction of 2-chloroethyl ethyl sulfide by magnetic activated carbon from aqueous samples prior to gas chromatography-ion mobility spectrometry analysis. *Microchem. J.* **193**, 109146 (2023).
45. Almasi, S., Ghobadian, B., Dehghani Soufi, M., Kakavandi, B. & Aubin, J. Calcium oxide anchored on magnetic waste-based activated carbon (MAC@CaO): a sustainable green heterogeneous catalyst for bio-based fuel and lubricant production. *Biomass Bioenerg.* **182**, 107071 (2024).
46. Rouhani, M., Ashrafi, S. D., Taghavi, K., Joubani, M. N. & Jaafari, J. Evaluation of tetracycline removal by adsorption method using magnetic iron oxide nanoparticles (Fe3O4) and clinoptilolite from aqueous solutions. *J. Mol. Liq.* **356**, 119040 (2022).
47. Pavia, D. L., Lampman, G. M., Kriz, G. S. & Vyvyan, J. A. Introduction to spectroscopy: Cengage learning; (2014).
48. de la Luz-Asunción, M. et al. Non-linear modeling of kinetic and equilibrium data for the adsorption of hexavalent chromium by carbon nanomaterials: dimension and functionalization. *Chin. J. Chem. Eng.* **27** (4), 912–919 (2019).
49. Qureshi, T., Memon, N., Memon, S. Q., Abro, K. & Shah, S. W. LC/UV determination of cefradine, cefuroxime, and cefotaxime in dairy milk, human serum and wastewater samples. *SpringerPlus.* **2** (1), 1–8 (2013).
50. Moghaddam, N. S. M. et al. Application of magnetic activated carbon coated with CuS nanoparticles as a new adsorbent for the removal of tetracycline antibiotic from aqueous solutions (isotherm, kinetic and thermodynamic study). *Desalination Water Treat.* **280**, 297–311 (2022).
51. Danalıoğlu, S. T., Bayazit, Ş. S., Kuyumcu, Ö. K. & Salam, M. A. Efficient removal of antibiotics by a novel magnetic adsorbent: magnetic activated carbon/chitosan (MACC) nanocomposite. *J. Mol. Liq.* **240**, 589–596 (2017).
52. Hu, W., Niu, Y., Shen, T., Dong, K. & Wang, D. Magnetic biochar prepared by a dry process for the removal of sulfonamides antibiotics from aqueous solution. *J. Mol. Liq.* **400**, 124576 (2024).
53. Drenkova-Tuhtan, A. et al. Reusable and inductively regenerable magnetic activated carbon for removal of organic micropollutants from secondary wastewater effluents. *Water Res.* **255**, 121525 (2024).

Acknowledgements
The authors would like to express their appreciation to the Kerman University of Medical Sciences [Grant number 99001162] for supporting the current work.

Author contributions
A.R & M.D: designed the model and carried out the experiments. S.A: conceived the original idea, supervised the project and prepared the manuscript. H.R, Z.MF, H.N & T.S: contributed to interpreting the results and developing the method. All authors discussed the results and contributed to the final manuscript.

Funding
This work received a grant from the Kerman University of Medical Sciences [Grant number 99001162].

Declarations

Competing interests
The authors declare no competing interests.

Ethical approval
The Ethics Committee of Kerman University of Medical Sciences approved the study (IR.KMU.REC.1400.515).

Additional information
Correspondence and requests for materials should be addressed to M.D. or S.A.

Reprints and permissions information is available at www.nature.com/reprints.

Publisher's note Springer Nature remains neutral with regard to jurisdictional claims in published maps and institutional affiliations.